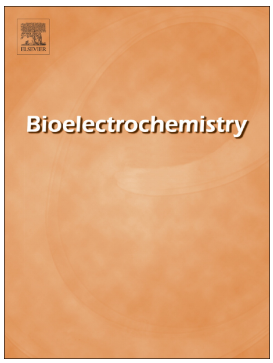

A hydrophobin-based-biosensor layered by an immobilized lactate dehydrogenase enzyme for electrochemical determination of pyruvate

Fatemeh Mirzaei, Mohammad Mirzaei, Masoud Torkzadeh-Mahani

PII: S1567-5394(19)30057-X
DOI: https://doi.org/10.1016/j.bioelechem.2019.06.008
Reference: BIOJEC 7323

To appear in: *Bioelectrochemistry*

Received date: 20 January 2019
Revised date: 24 June 2019
Accepted date: 24 June 2019" role="suppressed

Please cite this article as: F. Mirzaei, M. Mirzaei and M. Torkzadeh-Mahani, A hydrophobin-based-biosensor layered by an immobilized lactate dehydrogenase enzyme for electrochemical determination of pyruvate, Bioelectrochemistry, https://doi.org/10.1016/j.bioelechem.2019.06.008

A hydrophobin-based-biosensor layered by an immobilized lactate dehydrogenase enzyme for electrochemical determination of pyruvate

Fatemeh Mirzaei[a,b], Mohammad Mirzaei[b], Masoud Torkzadeh-Mahani[c*]

a. Department of Chemistry, Shahid Bahonar University of Kerman, Kerman, Iran

b. Young Research Society, Shahid Bahonar University of Kerman, Kerman, Iran

c. Department of Biotechnology, Institute of Science, High Technology and Environmental Science, Graduate University of Advanced Technology, Kerman, Iran

Abstract

Appropriate enzyme immobilization on the electrode surface in order to access its active site has always been an important strategy for electrode modification. In this report, lactate dehydrogenase enzyme was appropriately immobilized on the glassy carbon electrode via hydrophobin (HFB1) and graphene oxide nanocomposite. The step-by-step modification was successfully confirmed by water contact analysis, cyclic voltammetry, and electrochemical impedance spectroscopy. Under optimum conditions, this biosensor demonstrated a detection limit of 8.69 nM and RSD of 4.3% and 3.6% (n=5) for reproducibility and repeatability. The effect of scan rate on the oxidation behavior of NADH was investigated by cyclic voltammetry; and diffusion coefficient for NADH was estimated at 6.27×10^{-8} $cm^2.s^{-1}$. The apparent Michaelis–Menten constant (K_m^{app}) was amperometrically determined and it was lower than K_m^{app} for the free enzyme. Also, the modified electrode represented good stability after nine days with 6% decrease in current. The proposed assay was successfully used in real sample-serum-analysis and the obtained recoveries were between 93% and 104.0%.

Graphical abstract

*Corresponding author: Department of Biotechnology, Institute of Science, High Technology and Environmental Science, Graduate University of Advanced Technology, Kerman, Iran, Postal code: 7616914111, Email:mtmahani@gmail.com

Keywords: Graphene nanocomposite, Hydrophobin, Pyruvate determination, Lactate dehydrogenase enzyme

Highlights

- A selective LDH nanobiosensor was fabricated for pyruvate determination.
- GO nanocomposite increased current response.
- GO nanocomposite helped increasing hydrophobicity of the electrode surface.
- Hydrophobin helped suitable attachment of the enzyme to the electrode surface.
- Hydrophobin helped the enzyme stability.
- This fabricated biosensor exhibited good selectivity, stability, and reproducibility.

1. Introduction

Pyruvate, the conjugate base of pyruvic acid, is an important intermediate in several metabolic pathways and participates in different biochemical reactions. Therefore, its levels in the blood can be used as a biochemical index for the severity of circulatory disorder [1]. The high pyruvate concentration in blood demonstrate the PDHC (pyruvate dehydrogenase complex) deficiency, which thereby results in inadequate removal of pyruvate and generation of lactate leading to insufficient energy production. Thereby, increased levels of pyruvate are known to play a prominent role in autism [2]. In addition, in the food industry, it serves as an index of bacterial contamination of various media, such as dairy products [3]. Different methods have been reported for pyruvate detection such as spectrophotometric analyses [4], fluorometric assay [5, 6], infrared spectroscopy [7], liquid chromatography [1], and electrochemical methods[8] [9].

In recent years, electrochemical methods using biosensors have attracted considerable attention due to their unique merits. In comparison with other techniques, electrochemical methods are fast, low cost, simple, sensitive, and selective. Electrochemical biosensors enjoy the advantages of both electrochemical biosensing and nanotechnology. Polyvinyl alcohol (PVA) is a good choice for the preparation of polymer nanocomposites because of its biocompatibility and water solubility. PVA based nanocomposites with metal nanoparticles[10] and carbon-based nanomaterials[11] as nanofillers have been synthesized. This combination has superior mechanical and thermal properties. Also, the strong interfacial interaction between PVA and graphene oxide /AuNPs leads to the better dispersion of the composite. Graphene oxide as a nanomaterial has been employed in

various electrochemical biosensors because of its significant surface area-to-volume ratio, generation of high signal intensity, and unique facility for electrode modification. Furthermore, excellent electrocatalytic activity has been achieved for NADH detection by graphene-based electrochemical biosensors [12, 13].

The immobilization of the enzyme on electrochemical sensors has become a generally acknowledged issue in biosensing methods. To improve enzyme efficiency and for better immobilization, hydrophobins can be a good candidate. Hydrophobins are fungi proteins consisting of almost 100 amino acids, and considered one of the most active of surface active proteins [14]. They are secreted by filamentous fungi and have different functions in fungal physiology related to surface phenomena, including adhesion, the formation of surface layers, and reduction of surface tension [15]. One of the most multipotent characteristics of these proteins is self-assembly in to hydrophobic/hydrophilic interfaces [16], contributing to their use as a material surface modifying and enzyme and cell adsorbing agent [17]. Hydrophobins have been applied to enzyme stabilization [18], biosensor [19] and electrode modification [20], drug delivery [21, 22], and surface coating [23, 24]. Hydrophobin utilization for enzyme immobilization on an electrode surface has been reported for glucose oxidase [14] and choline oxidase [25], indicating good immobilization and excellent stability.

Herein, a biosensor based on graphene oxide/Au nanoparticle (NPs)/poly (vinyl alcohol) (PVA), hydrophobin, and lactate dehydrogenase enzyme has been fabricated for pyruvate determination. The newly synthesized nano-composite (GO/AuNPs/PVA) showed that HFB1 (hydrophobin HFB1) was immobilized on the modified electrode surface through its hydrophobic head and, therefore, this assembly was suitable for the immobilization of LDH enzyme via hydrophilic interaction to access the active site of the enzyme. Pyruvate could then be measured by evaluating the decrease in NADH co-factor concentration.

2. Experimental

2.1. Chemicals

Lactate dehydrogenase enzyme and HFB1 protein were recombinantly produced in our laboratory [26]. Other chemicals were of analytical grade and purchased from Sigma

Aldrich. Human serum (with ethical permission: IR.KMU.REC.1398.22) was used for real sample analysis.

2.2. Instruments

The morphology of the synthesized graphene oxide (GO) and GO/AuNPs/PVA composite was evaluated by using a KYKY EM3200 scanning electron microscope (SEM). The FT-IR spectrum was recorded on an FT-IR spectrometer (Brucker, model Tensor 27). The X-ray diffraction (XRD) patterns of the synthesized graphene oxide were obtained on an X'PertPro (Holland). The ultraviolet-visible spectrum was recorded by a Cary 50 UV−vis spectrophotometer (Varian, USA), equipped with 1.0cm quartz cells. Moreover, electrochemical measurements were performed using a Portable Bipotentiostat/Galvanostat µStat 400, controlled by Drop View software, interfaced with a personal computer for potential control and collecting data. A three-electrode system, including a glassy carbon electrode (GCE) with a diameter of 2 mm as the working electrode, Ag/AgCl as the reference electrode, and a platinum wire as the counter electrode, were employed. Impedance measurements were performed with an Autolab potentiostat/galvanostat (PGSTAT 302 N, Eco Chemie, the Netherlands). Finally, a pH meter (Metrohm 713) was used to measure the pH of the solution.

2.3. Synthesis of Graphene Oxide (GO), AuNPs, and Nanocomposites

Graphene oxide was synthesized by a modified Hummer's method [27]. Briefly, 120 ml of concentrated H_2SO_4 solution was mixed with 5 g of graphite powder in a round-bottom flask, and the mixture was allowed to stir for 10 min. Next, 2.5 g of $NaNO_3$ was added to the previous mixture (mild pre-oxidation step). After that, the temperature was reduced using an ice bath, and then 15 g of KMnO4 was added to the mixtureover three hours. The mixture which was stirred for for four days. In the next step, 700 ml of water and 40 ml of H_2O_2 solution (30%) were added to the mixture and it was stirred for one day to obtain the graphite oxide mixture which was later centrifuged and washed four times with HCl solution (5% v/v) and then repeatedly washed with water until the pH of the solution became neutral. Finally, the resulting solution was sonicated for 60 min. The graphene oxide precipitate was obtained by drying in a vacuum.

AuNPs were prepared according to the citrate reduction protocol [28]. According to the Beer-Lambert law , A=εbc, where A is absorbance at 520 nm (here, 0.81), ε is the molar absorption coefficient of AuNPs at 520 nm (4.2×10^{8} $M^{-1}cm^{-1}$), b is the path length of the absorbing medium (here, 1 cm), c, the concentration of AuNPs, was obtained as 1.9 nM (Fig. 1 A).

For the preparation of the graphene oxide AuNPs composite (GO/AuNPs), a specified volume of AuNPs was added to GO powder and allowed to stir for one day. Afterwards, the solvent was evaporated in an oven at 70 °C for 12 hours.

To prepare the PVA/GO/AuNPs nanocomposite, PVA was dissolved in deionized water at 80 °C in a three-neck flask and stirred to obtain an aqueous solution. Then, the GO/AuNPs aqueous suspension was dripped into the PVA solution and was allowed to stir for five hours at 80 °C [29]. Cyclic voltammetry as illustrated in Fig. 3 A and B. gave the optimum ratio of PVA to GO/AuNPs.

2.4. Preparation of the Electrochemical Biosensors

The GCE was polished using 0.05 μm of alumina powder for 15 min, followed by ultrasonication in water and ethanol. In the next step, it was transferred to the electrochemical cell for further cleaning and activation via cyclic voltammetry between −1.5 V and +1.5 V at a scan rate of 100 mV s^{-1} in 0.5 $mol.L^{-1}$ of freshly prepared deoxygenated H_2SO_4 until a stable cyclic voltammetric profile (≈10 times) was obtained. The pretreated electrode was dried at room temperature. After that, 5 μL of the GO/AuNPs/PVA suspension was dropped on the electrode surface and air-dried until a uniform film was formed. Next, the modified electrode was immersed in 30 μg/ml of HFB1 solution for 12 hours at 4 °C. Then, 5 μL of the LDH enzyme (0.01 mg/ml) was drop-caste on the surface of the modified electrode with GO/AuNPs/PVA-HFB1. The modified electrode was stored at 4 °C at constant humidity condition when not in use.

2.5. The principle of biosensor

As displayed in the sensing mechanism of the modified electrode (Schematic 1), HFB1 acts as a glue to immobilize the enzyme on the electrode surface. Since it was more important to access the active site of the enzyme, hydrophobin was immobilized

on the electrode surface via the hydrophobic side. Therefore, to providing a hydrophobic surface for the stable immobilization of hydrophobin, the GO/AuNPs/PVA nanocomposite acts as a direct electrochemical connector between the electrode surface and the redox center of the LDH and, therefore, facilitates the electron transfer. Pyruvate can be estimated by evaluating the decrease in NADH cofactor concentration according to the stoichiometric relationship in the following reaction:

$$\text{Pyruvate} + \text{NADH} \overset{\text{LDH}}{\underset{2H^+\ 2e}{\Longleftrightarrow}} \text{Lactate} + \text{NAD}^+ \qquad (1)$$

Schematic 1

The equilibrium constant of this reaction at pH 7.4 is very large (10^4). Thus, the reaction proceeded from left to right and could be considered almost irreversible [30].

3. Results and Discussion

3.1. Characterization of Nanocomposite

As evident from the FT-IR spectrum of the prepared graphene oxide (Fig. 1 B), the characteristic band at 1031.54 cm^{-1} was assigned to C-O alkoxy stretching, and the band at 1666.02 cm^{-1} indicated the stretching vibration of C=O. In addition, an O-H stretching vibration was observed around 3420 cm^{-1}.

Fig. 1

The XRD pattern of the synthesized graphene oxide is illustrated in Fig. 1C. A peak around 2theta = 10.6 in the XRD pattern confirmed that GO was successfully exfoliated, and this peak belonged to the interlayer of 8.32 Å. A similar peak around 10.6 in the XRD pattern was reported by Gupta et al. for GO synthesized by modified Hummer's method [31]. As indicated in the SEM image of the GO and GO/AuNPs/PVA nanocomposite (Fig. 2), a very thick layer of GO was prepared (A), and a layer of AuNPs was formed on the GO surface (B).

Fig. 2

3.2. Wettability of Different HFB1-Modified GCEs Surfaces

The water contact angle was used to evaluate the wettability of glassy carbon electrode surface before and after modification with HFB1.Fig.3 shows that water contact angle of the bare glassy carbon electrode surface increased from 60.3^0 ($\pm$ 2.4^0) to 73.6^0 ($\pm$ 1.2^0) (n=3) after modification with GO/AuNPs/PVA and the hydrophobicity of the electrode surface was increased (B). In the next step of the modification, the water contact angle of the electrode surface remarkably decreased to 21.7^0 $\pm$ 2.0^0 indicating that HFB1 immobilized on the GO/AuNPs/PVA modified the electrode by the hydrophobic side and therefore the hydrophilicity of the surface was significantly increased (C). The hydrophobicity of the surface after the next modification with LDH (giving a water contact angle of 36.9^0 $\pm$ 2.7^0) proved that the enzyme immobilized in a suitable orientation and its active site was accessible (D) [32].

Fig. 3

3.3. The Characterization of the stepwise electrode modification

Cyclic voltammograms were recorded at different steps of nanocomposite and enzyme immobilization on the electrode surface in l mM $Fe(CN)_6^{3-/4-}$ solution. The results are presented in Fig. 4A. It is clear that a pair of well-defined redox peaks with a peak-to-peak separation (ΔE_p) of 0.51 V was observed for bare glassy carbon electrode corresponding to $Fe(CN)_6^{3-/4-}$. After electrode surface modification with GO composite, the current significantly increased and the ΔE_p slightly decreased to 0.15 V. Also, an increase was observed in current after modification of the bare glassy carbon with GO/AuNPs due to increased surface area. Therefore, the oxidation/reduction of $Fe(CN)_6^{3-/4-}$ became facile on the GO/AuNPs glassy carbon electrode. In comparison with the GO/AuNPs modified glassy carbon electrode, the electrode surface modified with GO/AuNPs/PVA showed a decrease in current. After incubating the GO/AuNPs/PVA electrode in HFB1 solution, the voltammetric peak current clearly decreased and ΔE_p increased, indicating immobilization of the enzyme on the GO/AuNPs/PVA/HFB1 electrode surface and hindering diffusion. Finally, after LDH immobilization, the peak current was also reduced, providing the immobilization of the

enzyme on the GO/AuNPs/PVA/HFB1 electrode surface and hindered it. The Nyquist plots of stepwise electrode modification are shown in Fig. 4B. The results indicate that the diameter of the impedance semicircle GO/AuNPs electrode is less than that of the GO electrode, exhibiting a lower electron-transfer resistance and higher conductivity. For the GO/AuNPs/PVA electrode, the electron-transfer resistance was increased. It was clear that the diameter of the semicircle increased consecutively with the successive self-assembly of HFB1 and the deposition of LDH, suggesting that the electron-transfer resistance increased step by step. The results were in good agreement with the results of the cyclic voltammograms.

Fig. 4

3.4. Optimization of Experimental Parameters for NADH Determination

To obtain high performance for biosensor sensing, the percentage of GO/AuNPs and PVA, pH of the electrolyte solution, type of buffer and its concentration were optimized. To obtain an optimum percentage of GO/AuNPs/PVA nanocomposite, at a constant percentage (2.5%) of PVA, four composites with variable percentages of the GO/AuNPs were synthesized. The glassy carbon electrode modified with each of these and their related cyclic voltammograms in 1mM $Fe(CN)_6^{3-/4-}$ solution were recorded. As depicted in Fig. 5(A), both current and the potential approached a plateau at a a percentage of 5; therefore, 5% was determined as optimum. Also, the optimum percentage for PVA was 2.5% at a constant percentage of GO/AuNPs (5%) and a variable percentage of PVA, as indicated in Fig. 5 (B). The influence of pH on the oxidation peak of NADH was investigated in Britton–Robinson (B.R.) buffer in the PH range 2-9. According to Fig. 5 (C), as the pH increased from 2 to 7, the anodic peak current for NADH increased. Furthermore, the potential of the anodic peak shifted to a more positive potential. After pH7, the current of anodic peak decreased and this pH was selected as the optimum. The buffer and its concentration were selected as PBS buffer and 0.1 M based on Fig. 5 (D, E).

Fig. 5

3.5. The Effect of scan Rate on Biosensor Performance

The electrochemical behavior of the GO/AuNPs/PVA/HFB1 glassy carbon electrode with increasing scan rates was investigated by cyclic voltammetry in 0.01M NADH solution. As indicates that Fig. 6A, the anodic peak current of NADH increased with adding the scan rate between 0.01 to 0.1 $V.s^{-1}$, the anodic peak potential shifted to more positive potentials, and no cathodic peak was represented. Fig. 6 B indicated that the oxidation peak of NADH increases linearly with the square root of the scan rate with a regression coefficient of 0.987, illustrating that the electrocatalytic process was controlled by the diffusion of the electroactive species from the solution to the redox site of the electrode [33]. Using the slope of the plot of the anodic peak current vs. the square root of scan rate and the Randles-Sevcik equation for totally irreversible electron transfer, the electron transfer coefficient for NADH was computed as follows:

$$i_p = (2.99 \times 10^5)\, n\, \alpha^{0.5}\, A\, C^*\, D^{0.5}\, \upsilon^{0.5} \qquad (2)$$

where n denotes the number of exchanged electrons, α represents the electron transfer coefficient, A indicates the surface area of the working electrode, C* and D respectively are the bulk concentration and diffusion coefficients of the electroactive species, and υ is the potential scan rate. Moreover, α was obtained as 0.44 by the slope of the E_{pa} versus log υ (Fig. 6 C) [34]. The diffusion coefficient of NADH was found to be 6.27×10^{-8} $cm^2.s^{-1}$.

Fig. 6

3.6. Analytical Performance Characteristics by DPV and Amperometry Techniques

Fig. 7 A gives an overview of the oxidation of NADH in 0.1M PBS buffer (pH=7) by differential pulse voltammetry at the GO/AuNPs/PVA/HFB1/LDH glassy carbon electrode. Based on the voltammograms, the oxidation peak potential of NADH was 0.73 V and the anodic peak current was decreased by adding pyruvate. The difference between the anodic peak current before and after pyruvate addition (Δi_{pa}) was linear with pyruvate concentration (Fig. 7 B). The regression equation was $\Delta i_{pa} = 6.9 \times 10^{-3}$

[Pyr] + 0.70 (R^2= 0.991), the linear range was 50 to 1200 nM, and the other regression equation of Δi_{pa}= 9.92×10^{-5} [Pyr] + 9.00 (R^2= 0.990) was obtained in the range of 5 to 140 μM.

The limit of detection and the limit of quantification of the biosensor were estimated to be 8.69 nM and 20.90 μM respectively. Compared with some reported detection limits given in Table 1, the proposed method showed a lower detection limit with a wider linear range.

Table 1

In order to determine the apparent Michaelis-Menten constant (K_m^{app}), the amperometry technique was employed. The amperometric response inNADH solution (10 mM) by the addition of different amounts of pyruvate into a stirred 0.1M PBS buffer solution (pH=7) on a GO/AuNPs/PVA/HFB1/LDH glassy carbon electrode at 0.7 V operating potential vs Ag/AgCl is illustrated in Fig. 7 C. According to the data provided, a decrease in the amperometric current was produced for each successive increase of 0.05mM pyruvate. In the differential pulse voltammograms shown in Fig. 7 A, a similar trend could be observed. The apparent Michaelis–Menten constant was calculated from the slope and the intercept of the plot of the reciprocal steady-state current versus reciprocal pyruvate concentration (Fig. 7 D, inset) according to the Lineweaver-Burk equation[35]:

$$\frac{1}{i_{ss}} = \left(\frac{K_m^{app}}{i_{max}}\right)\left(\frac{1}{C}\right) + \left(\frac{1}{i_{max}}\right) \qquad (3)$$

where i_{ss} and i_{max} are the currents measured for enzymatic pyruvate detection under conditions of steady-state and NADH saturation, respectively, and C is the NADH concentration. The K_m^{app} of LDH immobilized on the modified electrode was calculated to be 1.5 mM, which was lower than the value estimated for free LDH (4.0 mM). Using HFB1 as modifier caused the enzyme be stable. The Km of immobilized LDH was lower, indicating higher affinity for LDH after immobilization [14].

Fig. 7

3.7. Selectivity, Reproducibility, and Stability of biosensor

To demonstrate the selectivity of pyruvate detection, the effect of ascorbic acid (AA), citric acid (CA), and glucose as the main interference under biological conditions was investigated on the anodic peak current response to pyruvate by a GO/AuNPs/PVA/HFB1/LDH glassy carbon electrode in 0.1M PBS buffer solution (pH=7) (Fig. 8 A). The addition of AA, CA, and glucose solution (150 µM) did not have a significant influence on the current response to pyruvate solution (1.5 µM). This result is one of the advantages of the fabricated biosensor, providing highly selective detection for pyruvate.

To evaluate the reproducibility of the GO/AuNPs/PVA/HFB1/LDH glassy carbon electrode, the DPVs of five electrodes were recorded for NADH detection under the same condition (Fig. 8 B). A good reproducibility with a relative standard deviation (RSD) of 4.3% was obtained. The repeatability with RSD was also estimated at 3.6 % with five independent DPVs measurements.

Furthermore, the stability of the biosensor was investigated over 15 days as depicted in Fig. 5 C. When the sensor was not in use, it was stored at 4 $^{\circ}$C. After nine days, the anodic peak current was 94% of the initial current and, after two weeks, the anodic peak current was 85% (Fig. 8 C). These results indicated that the biosensor had excellent selectivity and good stability for pyruvate determination.

Fig. 8

3.8. Pyruvate Detection in the Real Sample

The application of the biosensor was successfully performed in three real samples (serum) after appropriate pretreatment. The recovery of this assay was calculated by the standard addition method. Based on Table 2, the recovery was in the range of 93-104. Therefore, this biosensor was appropriate for real sample analysis.

Table 2.

4. Conclusion

Using the GO/AuNPs/PVA composite, an increase in the electrode current response was observed due to an increase in the surface-to-volume ratio and high electrical conductivity. In addition, the hydrophobicity of the electrode surface was enhanced after the immobilization of the GO composite. Consequently, the appropriate self-assembly of HFB1 for the immobilization of LDH was observed and proven by water contact angle of the electrode surface. HFB1 not only caused LDH to be immobilized through the hydrophilic head on the electrode surface but also improved the enzyme stability. This electrochemical biosensor demonstrated an acceptable precision, storage stability, and reproducibility, as well as a low detection limit and wide linear range in comparison to the other previously reported sensors. Finally, the enzyme biosensor was successfully applied to real sample analysis.

Acknowledgments

The financial support of the Research Council of Shahid Bahonar University of Kerman (grant number: of M/342/41) and the Institute of Science, High Technology & Environmental Science, Graduate University of Advanced Technology of Kerman is gratefully acknowledged.

References

[1] C.-K. Chuang, T.-J. Wang, C.-Y. Yeung, D.-S. Lin, H.-Y. Lin, H.-L. Liu, H.-T. Ho, W.-S. Hsieh, S.-P. Lin, A method for lactate and pyruvate determination in filter-paper dried blood spots, J. Chromatogr. A, 1216 (2009) 8947-8952.https://doi.org/10.1016/j.chroma.2009.10.074

[2] M. Malik, R. Chaudhary, C.S. Pundir, An improved enzyme nanoparticles based amperometric pyruvate biosensor for detection of pyruvate in serum, Enzyme and Microbial Technology, 123 (2019) 30-38.https://doi.org/10.1016/j.enzmictec.2019.01.006

[3] T. Pérez-Ruiz, C. Martínez-Lozano, V. Tomás, J. Fenoll, Chemiluminescence determination of citrate and pyruvate and their mixtures by the stopped-flow mixing technique, Anal. Chim. Acta, 485 (2003) 63-72.https://doi.org/10.1016/S0003-2670(03)00402-1

[4] V.H. Beretta, F. Bannoud, M. Insani, C.R. Galmarini, P.F. Cavagnaro, Variability in spectrophotometric pyruvate analyses for predicting onion pungency and nutraceutical value, Food Chem., 224 (2017) 201-206.https://doi.org/10.1016/j.foodchem.2016.12.031

[5] A. Zhu, R. Romero, H.R. Petty, A sensitive fluorimetric assay for pyruvate, Anal. Biochem., 396 (2010) 146-151.https://doi.org/10.1016/j.ab.2009.09.017

[6] F. Shapiro, N. Silanikove, Rapid and accurate determination of malate, citrate, pyruvate and oxaloacetate by enzymatic reactions coupled to formation of a fluorochromophore: Application in colorful juices and fermentable food (yogurt, wine) analysis, Food Chem., 129 (2011) 608-613.https://doi.org/10.1016/j.foodchem.2011.04.074
[7] R. Tavallaie, Z. Talebpour, J. Azad, M.R. Soudi, Simultaneous determination of pyruvate and acetate levels in xanthan biopolymer by infrared spectroscopy: effect of spectral pre-processing for solid-state analysis, Food Chem., 124 (2011) 1124-1130.https://doi.org/10.1016/j.foodchem.2010.07.016
[8] D.Y. Kucherenko, I.S. Kucherenko, O.O. Soldatkin, Y.V. Topolnikova, S.V. Dzyadevych, A.P. Soldatkin, A highly selective amperometric biosensor array for the simultaneous determination of glutamate, glucose, choline, acetylcholine, lactate and pyruvate, Bioelectrochemistry, 128 (2019) 100-108.https://doi.org/10.1016/j.bioelechem.2019.03.010
[9] M.E. Ghica, C.M.A. Brett, Development of Novel Glucose and Pyruvate Biosensors at Poly(Neutral Red) Modified Carbon Film Electrodes. Application to Natural Samples, Electroanalysis, 18 (2006) 748-756.10.1002/elan.200503468
[10] S. Pandey, S.K. Pandey, V. Parashar, G.K. Mehrotra, A.C. Pandey, Ag/PVA nanocomposites: optical and thermal dimensions, J. Math. Chem., 21 (2011) 17154-17159.10.1039/C1JM13276H
[11] T.V. Panova, A.A. Efimova, A.V. Efimov, A.K. Berkovich, Physico-mechanical properties of graphene oxide/poly(vinyl alcohol) composites, Colloid and Polymer Science, (2019).10.1007/s00396-018-04465-3
[12] A. Gasnier, M. Laura Pedano, M.D. Rubianes, G.A. Rivas, Graphene paste electrode: Electrochemical behavior and analytical applications for the quantification of NADH, Sens. Actuators, B, 176 (2013) 921-926.https://doi.org/10.1016/j.snb.2012.09.092
[13] P.-P. Gai, C.-E. Zhao, Y. Wang, E.S. Abdel-Halim, J.-R. Zhang, J.-J. Zhu, NADH dehydrogenase-like behavior of nitrogen-doped graphene and its application in NAD+-dependent dehydrogenase biosensing, Biosens. Bioelectron., 62 (2014) 170-176.https://doi.org/10.1016/j.bios.2014.06.043
[14] Z.-X. Zhao, M.-Q. Qiao, F. Yin, B. Shao, B.-Y. Wu, Y.-Y. Wang, X.-S. Wang, X. Qin, S. Li, L. Yu, Q. Chen, Amperometric glucose biosensor based on self-assembly hydrophobin with high efficiency of enzyme utilization, Biosens. Bioelectron., 22 (2007) 3021-3027.https://doi.org/10.1016/j.bios.2007.01.007
[15] M. Linder, G.R. Szilvay, T. Nakari-Setälä, H. Söderlund, M. Penttilä, Surface adhesion of fusion proteins containing the hydrophobins HFBI and HFBII from Trichoderma reesei, Protein Sci, 11 (2002) 2257-2266
[16] T. Kudo, Y. Sato, T. Hara, T. Joh, Y. Tasaki, Heterogeneous expression and emulsifying activity of class I hydrophobin from Pholiota nameko, Mycoscience, 52 (2011) 283-287.https://doi.org/10.1007/S10267-010-0097-9
[17] L. Zhao, J. Liu, D. Song, X. Wang, F. Tai, H. Xu, M. Qiao, A visualized fusion protein based on self-assembly hydrophobin HGFI, Chem Res Chin Univ, 31 (2015) 781-786.10.1007/s40242-015-5135-x

[18] Y. Corvis, A. Walcarius, R. Rink, N.T. Mrabet, E. Rogalska, Preparing Catalytic Surfaces for Sensing Applications by Immobilizing Enzymes via Hydrophobin Layers, Anal. Chem., 77 (2005) 1622-1630.10.1021/ac048897w
[19] A. Piscitelli, A. Pennacchio, P. Cicatiello, J. Politi, L. De Stefano, P. Giardina, Rapid and ultrasensitive detection of active thrombin based on the Vmh2 hydrophobin fused to a Green Fluorescent Protein, Biosens. Bioelectron., 87 (2017) 816-822.https://doi.org/10.1016/j.bios.2016.09.052
[20] R. Bilewicz, J. Witomski, A. Van der Heyden, D. Tagu, B. Palin, E. Rogalska, Modification of Electrodes with Self-Assembled Hydrophobin Layers, J. Phys. Chem. B, 105 (2001) 9772-9777.10.1021/jp0113782
[21] X. Wang, J. Mao, Y. Chen, D. Song, Z. Gao, X. Zhang, Y. Bai, P.E.J. Saris, H. Feng, H. Xu, M. Qiao, Design of antibacterial biointerfaces by surface modification of poly (ε-caprolactone) with fusion protein containing hydrophobin and PA-1, Colloids Surf., B, 151 (2017) 255-263.https://doi.org/10.1016/j.colsurfb.2016.12.019
[22] L. Zhao, H. Xu, Y. Li, D. Song, X. Wang, M. Qiao, M. Gong, Novel application of hydrophobin in medical science: a drug carrier for improving serum stability, 6 (2016) 26461.10.1038/srep26461
[23] X. Zhang, S.M. Kirby, Y. Chen, S.L. Anna, L.M. Walker, F.R. Hung, P.S. Russo, Formation and elasticity of membranes of the class II hydrophobin Cerato-ulmin at oil-water interfaces, Colloids Surf., B, 164 (2018) 98-106.https://doi.org/10.1016/j.colsurfb.2018.01.017
[24] H.J. Hektor, K. Scholtmeijer, Hydrophobins: proteins with potential, Curr Opin Biotechnol., 16 (2005) 434-439.https://doi.org/10.1016/j.copbio.2005.05.004
[25] Z.-X. Zhao, H.-C. Wang, X. Qin, X.-S. Wang, M.-Q. Qiao, J.-i. Anzai, Q. Chen, Self-assembled film of hydrophobins on gold surfaces and its application to electrochemical biosensing, Colloids Surf., B, 71 (2009) 102-106.https://doi.org/10.1016/j.colsurfb.2009.01.011
[26] A. Lohrasbi-Nejad, M. Torkzadeh-Mahani, S. Hosseinkhani, Heterologous expression of a hydrophobin HFB1 and evaluation of its contribution to producing stable foam, Protein Expr Purif, 118 (2016) 25-30.https://doi.org/10.1016/j.pep.2015.09.025
[27] M.L. Yola, T. Eren, N. Atar, Molecularly imprinted electrochemical biosensor based on Fe@Au nanoparticles involved in 2-aminoethanethiol functionalized multi-walled carbon nanotubes for sensitive determination of cefexime in human plasma, Biosens. Bioelectron., 60 (2014) 277-285.https://doi.org/10.1016/j.bios.2014.04.045
[28] M. Dai, T. Huang, L. Chao, Q. Xie, Y. Tan, C. Chen, W. Meng, Horseradish peroxidase-catalyzed polymerization of l-DOPA for mono-/bi-enzyme immobilization and amperometric biosensing of H2O2 and uric acid, Talanta, 149 (2016) 117-123.http://dx.doi.org/10.1016/j.talanta.2015.11.047
[29] C. Bao, Y. Guo, L. Song, Y. Hu, Poly(vinyl alcohol) nanocomposites based on graphene and graphite oxide: a comparative investigation of property and mechanism, J. Math. Chem., 21 (2011) 13942-13950.10.1039/C1JM11662B
[30] S. Adachi, S. Tanabe, K. Hashimoto, Determination of pyruvate, L-lactate, and glutamic pyruvic transaminase by using an immobilized-lactate dehydrogenase column, Biotechnol. Bioeng., 26 (1984) 635-639.10.1002/bit.260260615
[31] R.K. Gupta, Z.A. Alahmed, F. Yakuphanoglu, Graphene oxide based low cost battery, Mater. Lett., 112 (2013) 75-77.https://doi.org/10.1016/j.matlet.2013.09.011

[32] X. Wang, H. Wang, Y. Huang, Z. Zhao, X. Qin, Y. Wang, Z. Miao, Q. Chen, M. Qiao, Noncovalently functionalized multi-wall carbon nanotubes in aqueous solution using the hydrophobin HFBI and their electroanalytical application, Biosens. Bioelectron., 26 (2010) 1104-1108.https://doi.org/10.1016/j.bios.2010.08.024
[33] J. Balamurugan, T.D. Thanh, N.H. Kim, J.H. Lee, Facile fabrication of FeN nanoparticles/nitrogen-doped graphene core-shell hybrid and its use as a platform for NADH detection in human blood serum, Biosens. Bioelectron., 83 (2016) 68-76.https://doi.org/10.1016/j.bios.2016.04.040
[34] R. Guidelli, G. Compton Richard, M. Feliu Juan, E. Gileadi, J. Lipkowski, W. Schmickler, S. Trasatti, Defining the transfer coefficient in electrochemistry: An assessment (IUPAC Technical Report), Pure and Applied Chemistry, 2014, pp. 245.
[35] R.A. Kamin, G.S. Wilson, Rotating ring-disk enzyme electrode for biocatalysis kinetic studies and characterization of the immobilized enzyme layer, Anal. Chem., 52 (1980) 1198-1205.10.1021/ac50058a010
[36] Y.-Y. Zhao, X.-F. Gao, Y.-S. Li, X. Ju, J. Zhang, J. Zheng, Determination of pyruvic acid by using enzymic fluorescence capillary analysis, Talanta, 76 (2008) 265-270.https://doi.org/10.1016/j.talanta.2008.02.031

Schematic 1. The steps for fabrication of LDH biosensor.

Fig. 1 (A) UV-vis absorption spectra for solution of AuNPs.(B) FT-IR spectrum and (C) XRD pattern of GO.

Fig. 2.SEM images of GO (A), and GO/AuNPs/PVA nanocomposite (B).

Fig. 3. Water contact angle of different steps of modified GCE surfaces, (A) bare GCE, (B) GO/AuNPs/PVAGCE, (C) GO/AuNPs/PVA/HFB1GCE and (D) GO/AuNPs/PVA/HFB1/LDH GCE.

Fig. 4 Cyclic voltammograms (A) and EIS (B) of bare and modified electrodes.(Pare blue bare electrode, yellow GOE, red GO/AuNPsE, green GO/AuNPs/PVAE, dark blue GO/AuNPs/PVA/HFB1E, purple GO/AuNPs/PVA/HFB1/LDHE)

Fig. 5. Variable percentage of GO/AuNPS with constant percentage of PVA (2.5%)(▲I_{pa} ,◊ E_{pa}) (A), variable percentage of PVA with constant percentage of GO/AuNPS (5%) (▲I_{pa} ,◊ E_{pa}) (B) for preparation of nanocomposite. The influence of pH on the peak current and potential of NADH oxidation in B.R. buffer in the pH range of 2 – 9 (▲ E_{pa},◊ ΔI) (C), investigation of buffer type in different buffer solution with concentration of 0.1 M (red tris, blue PBS, purple B.R., black citrate)(D) and the influence of PBS buffer concentration (green 0.01, orange 0.05, red 0.1, blue 0.15, purple 0.2). Error bars=±standard deviation and n=3.

Fig. 6. GO/AuNPs/PVA/HFB1GCE in 0.01M NADH in PBS buffer pH 7 at different scan rate (0.01, 0.02, 0.03, 0.04, 0.05, 0.06, 0.07, 0.08, 0.09, 0.1 V/s) (A), plot of current vs. square root of scan rate y= 31.193x -1.0861 R^2=0.987 (B), and plot of E_{pa} vs. log υ (y=0.0679x+0.9269 R^2=0.990) (C). Error bars=±standard deviation and n=3.

Fig.7. The differential pulse voltammograms of GO/AuNPs/PVA/HFB1/LDH glassy carbon electrode in 10 mM NADH solution before and after pyruvate addition (A), the plot of ΔIp_a vs. [Pyr] with two regression equation Δi_{pa}= 6.9 × 10^{-3} [Pyr] + 0.70 (R^2= 0.991), and Δi_{pa}= 9.92×10^{-5} [Pyr] + 9.00 (R^2= 0.990) . Error bars=±standard deviation and n=3 (B).The current – time response of modified electrode in 10 mM NADH solution before and after adding pyruvate with +0.7 V working potential (C), and the plot of I vs. [Pyr], (the inset was the plot of 1 / I versus 1 / [Pyr]) (E).

Fig. 8. The DPV responses of modified electrode after adding the Pyr, CA, AA, and glucose (A). Oxidation response of independently 5 fabricated biosensors (B) Stability of

the biosensor during 15 days (C) for NADH (10 mM) and pyruvate solution (0.5 µM) under optimum condition. Error bars = ±standard deviation and n=3.

Table 1 Response characteristics of different sensor for pyruvate determination.

Table 2 Pyruvate concentration in real sample with the proposed biosensor.

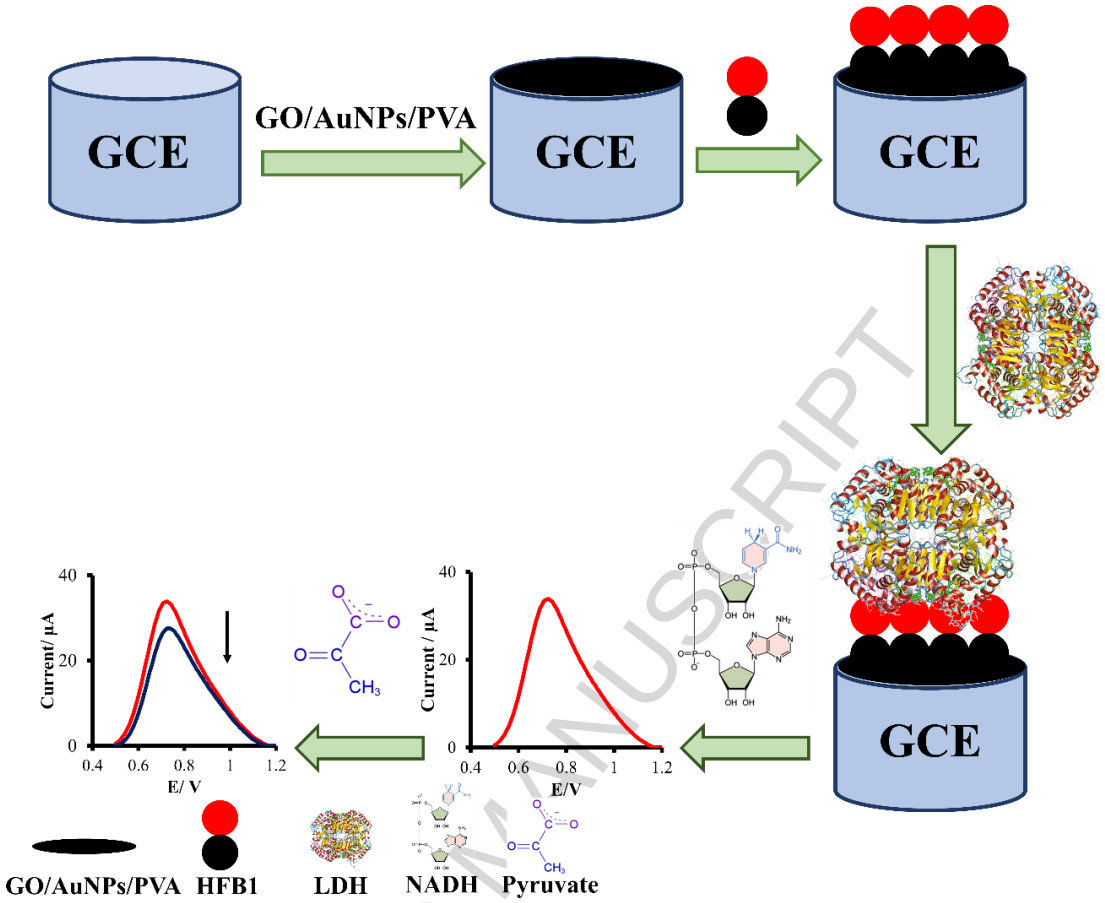

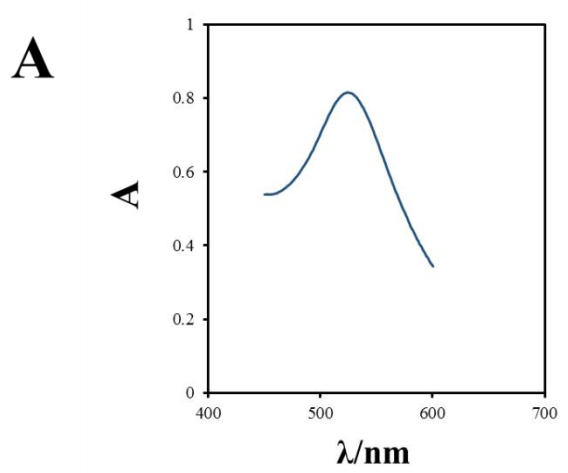

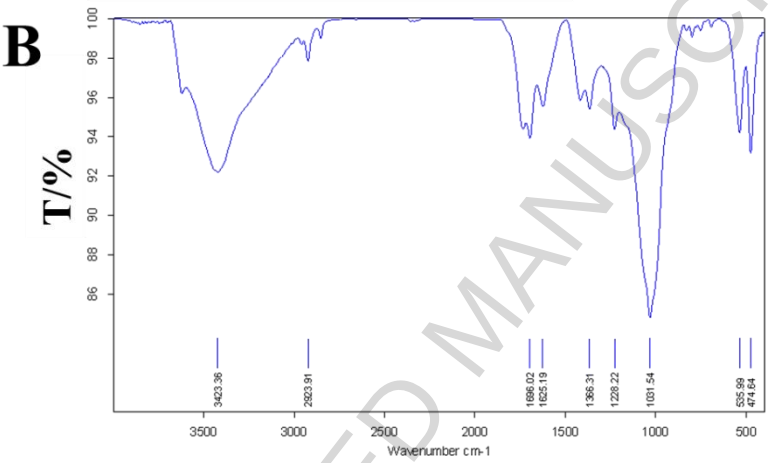

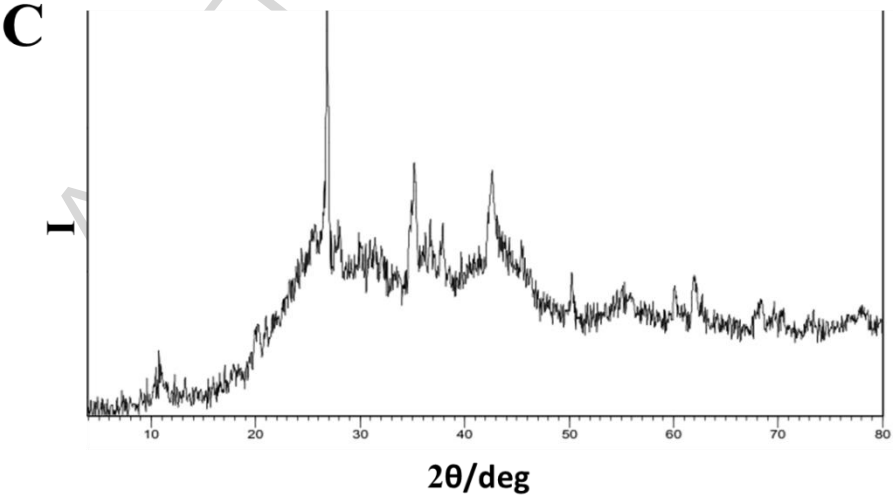

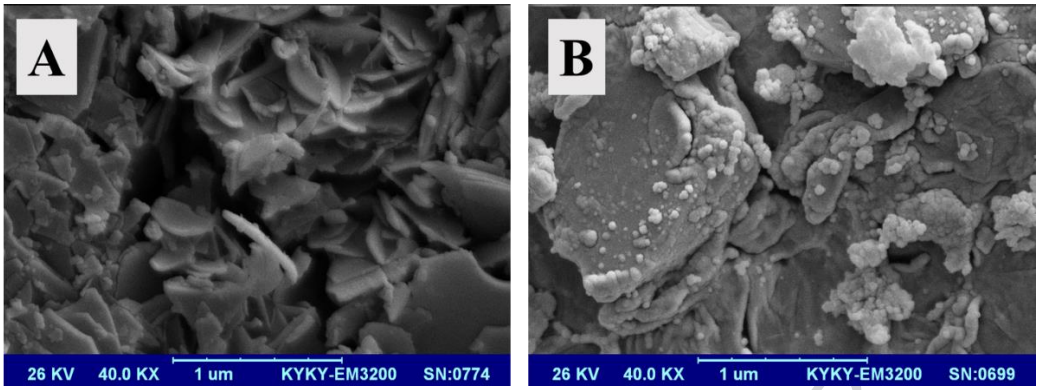

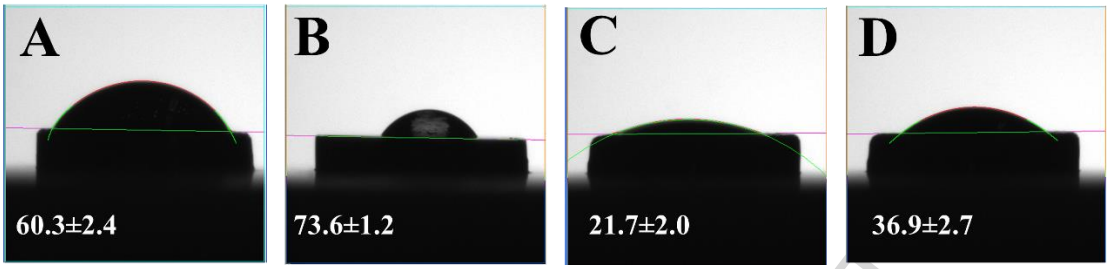

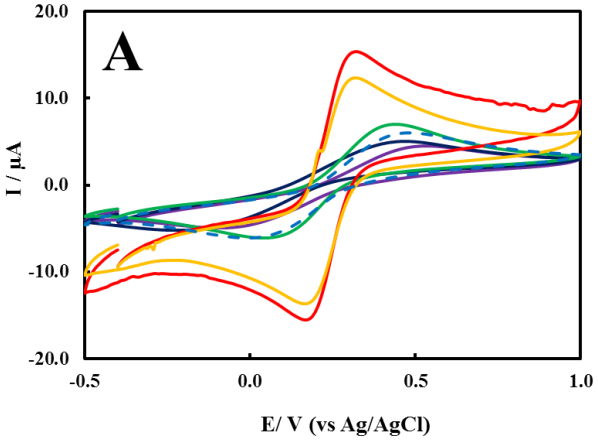

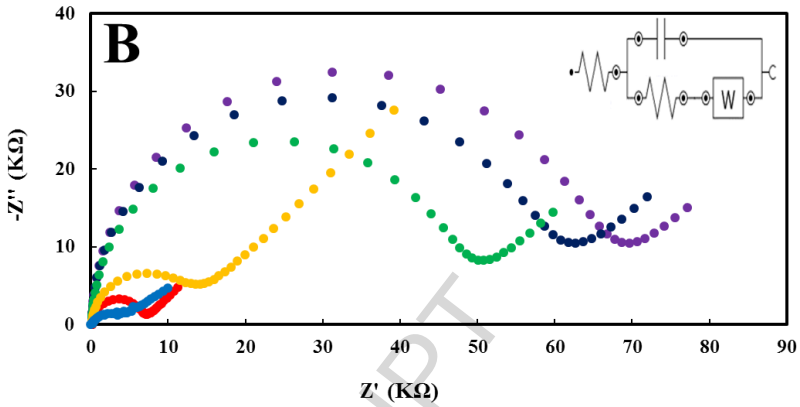

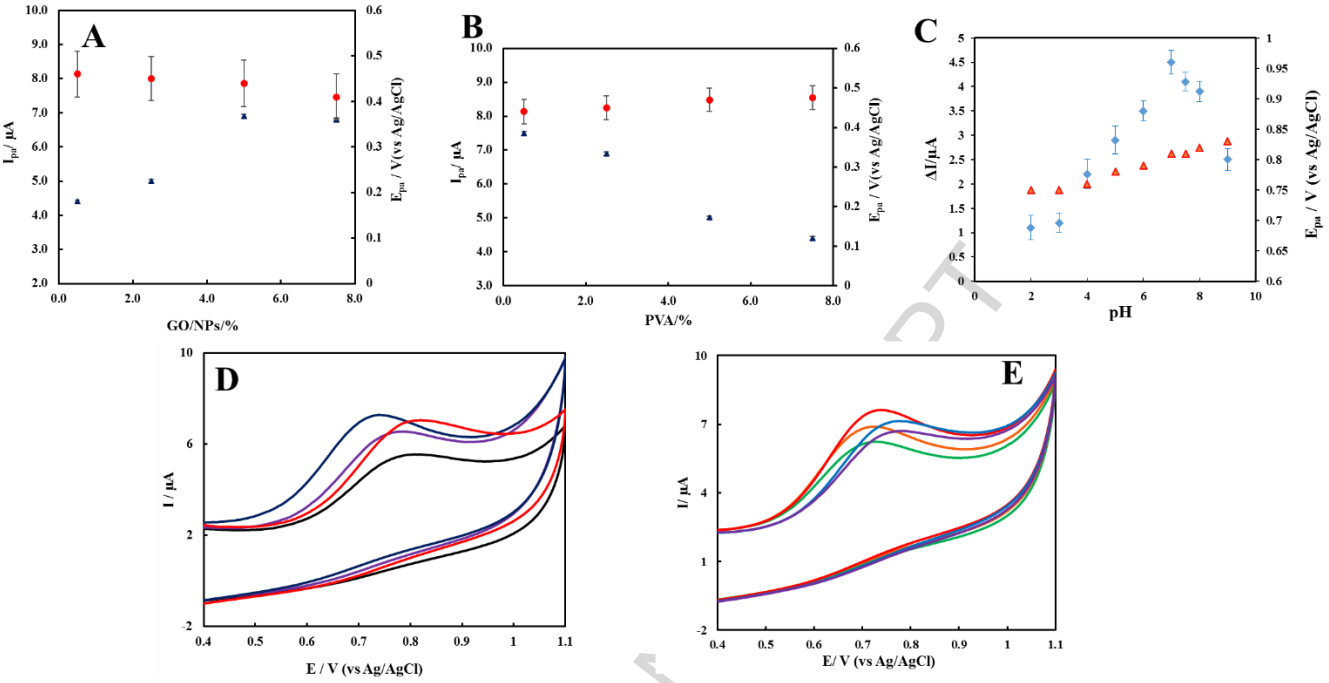

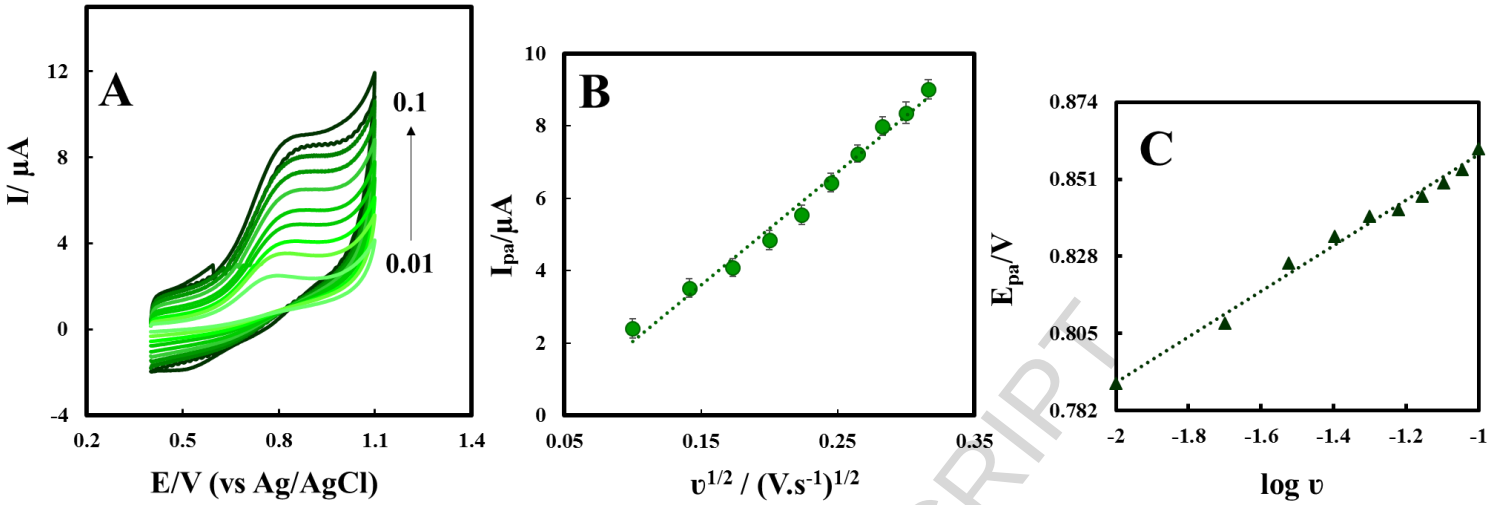

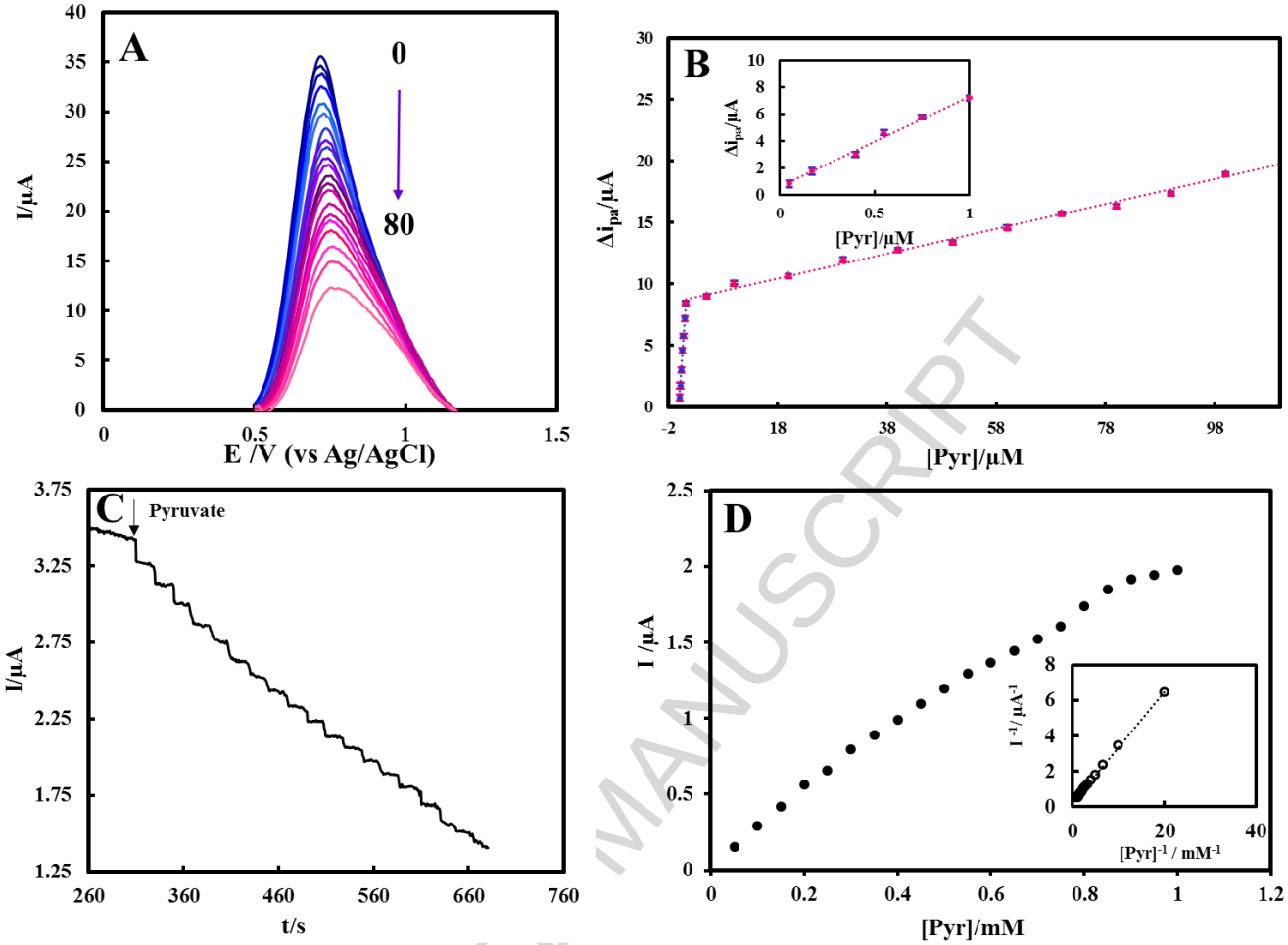

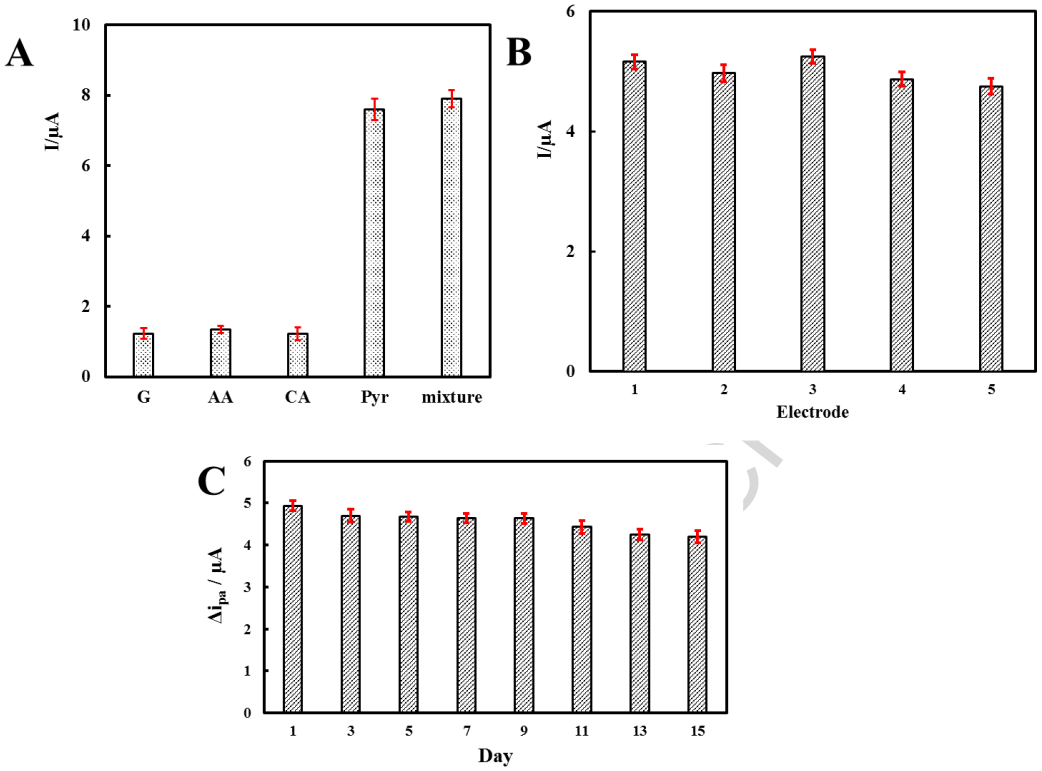

Method	DOE	Linear range (nM)	Ref.
Chemiluminescence	21.00 nM	$75.45 - 11.81\times10^{3}$	[3]
fluorimetric assay	5.00 nM	$0\text{-}1.00\times10^{3}$	[5]
Enzymic fluorescence capillary analysis	12.00 µM	$0.20\times10^{6}\text{-}1.20\times10^{6}$	[36]
Spectrophotometry: Schwimmer and Weston and Anthon and Barret protocol	Not mention	$1.00\times10^{4}\text{-}9.00\times10^{5}$	[4]
Fluorometric-coupled reaction	50.00 µM	$1.00\times10^{3}\text{-}1.00\times10^{6}$	[6]
Amperometric biosensors	34.00 µM	$9.00\times10^{4}\text{-}6.00\times10^{5}$	[9]
Electrochemical nanobiosensor	8.69 nM	$5.00\times10^{1}\text{-}1.20\times10^{3}$ $5\times10^{3}\text{-}1.40\times10^{5}$	This work

Sample	Initial $\times10^{2}$ (nM)	Added $\times10^{2}$ (nM)	Found $\times10^{2}$ (nM)	Recovery %
Serum 1	0.91	1.00	1.84	93.0
	0.91	4.00	4.77	96.5
Serum 2	7.53	1.00	8.47	94.0
	7.53	4.00	11.33	95.0
Serum 3	3.49	1.00	4.53	104.0
	3.49	4.00	7.33	96.0

Highlight

- A selective LDH nanobiosensor was fabricated for pyruvate determination.
- GO nanocomposite increased current response.
- GO nanocomposite helped increasing hydrophobicity of the electrode surface.
- Hydrophobin helped to the suitable attachment of the enzyme to the electrode surface.
- Hydrophobin helped the enzyme stability.
- This fabricated biosensor exhibited good selectivity, stability, and reproducibility.